Kinetics-based Inference of Environment-Dependent Microbial Interactions and Their Dynamic Variation

Hyun-Seob Song[1,2†]*, Na-Rae Lee[3†], Aimee K. Kessell[1], Seo-Young Park[4], Kang Zhou[5], and Dong-Yup Lee[4]*

[1]Department of Biological Systems Engineering, University of Nebraska-Lincoln, Lincoln, NE 68583

[2]Department of Food Science and Technology, Nebraska Food for Health Center, University of Nebraska-Lincoln, Lincoln, NE 68588

[3]Department of Bioscience and Biotechnology, Konkuk University, Seoul 05029, Republic of Korea

[4]School of Chemical Engineering, Sungkyunkwan University, Suwon-si, Gyeonggi-do 16419, Republic of Korea

[5]Department of Chemical and Biomolecular Engineering, National University of Singapore, 4 Engineering Drive 4, Singapore 117585, Singapore

[†]Both authors contributed equally.

*****Correspondence: hsong5@unl.edu (H.-S.S.); dongyuplee@skku.edu (D.-Y.L.)

ABSTRACT: Microbial communities in nature are dynamically evolving as member species change their interactions subject to environmental variations. Accounting for such context-dependent dynamic variations in interspecies interactions is critical for predictive ecological modeling. However, we lack a fundamental understanding of how microbial interactions are driven by environmental factors due to the absence of generalizable theoretical foundations, significantly limiting our capability to predict and engineer community dynamics and function. To address this issue, we propose a novel theoretical framework that allows us to represent interspecies interactions as an explicit function of environmental variables (such as substrate concentrations) by combining growth kinetics and a generalized Lotka-Volterra model. A synergistic integration of these two complementary models leads to the prediction of alterations in interspecies interactions as the outcome of dynamic balances between positive and negative influences of microbial species in mixed relationships. This unique capability of our approach was experimentally demonstrated using a synthetic consortium of two *Escherichia coli* mutants that are metabolically dependent (due to an inability to synthesize essential amino acids), but competitively growing on a shared substrate. The analysis of the *E. coli* binary consortium using our model not only showed how interactions between the two amino acid auxotrophic mutants are controlled by the dynamic shifts in limiting substrates, but also enabled quantifying previously uncharacterizable complex aspects of microbial interactions such as asymmetry in interactions. Our approach can be extended to other related ecological systems to model their environment-dependent interspecies interactions from growth kinetics.

IMPORTANCE: Modeling of environment-controlled interspecies interactions through separate identification of positive and negative influences of microbes in mixed relationships is a new

capability that can significantly improve our ability to understand, predict, and engineer complex dynamics of microbial communities. Moreover, robust prediction of microbial interactions as a function of environmental variables can serve as valuable benchmark data to validate modeling and network inference tools in microbial ecology, the development of which has often been impeded due to the lack of ground truth information on interactions. While demonstrated against microbial data, the theory developed in this work is readily applicable to general community ecology to predict interactions among microorganisms such as plants and animals, as well as microorganisms.

KEYWORDS: Microbial communities; competition; cooperation; context dependence; kinetic models; Lotka-Volterra models

INTRODUCTION

Microbial communities play pivotal roles in maintaining human and animal health, plant productivity, and ecosystem services (1-4). Increasing efforts are being dedicated towards maximizing their beneficial roles in natural systems or creating new industrial applications (5). However, control and design of microbial community dynamics and function is a challenging task, primarily due to higher-order or emergent properties that are not observable from individual species in isolation but arise through nonlinear interspecies interactions (6, 7). Therefore, rational design of microbial communities or consortia requires a fundamental knowledge of microbial interactions as a mechanistic linkage between the environment and the community compositions and function, necessitating the employment of predictive mathematical models as indispensable tools (8-14).

Development of accurate models of microbial communities that are commonly subject to environmental variations is truly complicated by the following intrinsic ecological aspects. First, microorganisms in a community build *dynamic* interactions that cannot effectively be represented by a rigid network with fixed structure (15, 16). Rather, microbial communities keep reorganizing interaction networks in response to biotic or abiotic perturbations or through adaptation to long-lasting environmental changes. Second, microorganisms often build *mixed* relationships by exerting *both* promotive and inhibitive impacts on the growth of their partners/neighbors (17, 18). Individual identification of these simultaneously acting positive and negative interactions is critical because community dynamics is mainly driven by the balances between all counteracting impacts among member species (19). The lack of capability to account for these key properties of microbial interactions limits our ability to predict and engineer microbial community dynamics and functions.

Despite rapid progress in microbiome science, we still do not know how to identify environment-controlled dynamic variation in interspecies interactions addressed above. Three major branches of microbial interaction modeling include (20, 21): (i) network inference, (ii) metabolic network modeling, and (iii) kinetic modeling. Network inference is widely used for modeling microbial interactions to identify interaction networks based on correlative relationships among microbial populations (22-25), parameter identification through regression (26-28), or a prescribed set of rules or hypotheses (21). The resulting networks represent interspecies interactions as single constant metrics, therefore being unable to describe dynamic variations in interactions nor identify the balances among counteracting individual impacts in mixed relationships. Recently, we developed the method termed MIIA (Minimal Interspecies Interaction Adjustment) (15, 16) to predict context-dependent interactions due to the changes in memberships, which however has not been extended to address the environmental impacts. In contrast with network inference, metabolic network and kinetic modeling can account for both positive and negative interactions based on cross-feeding of small molecules (essential for growth) or competition for shared substrates/nutrients among species; in theory, kinetic models can additionally simulate their dynamic variations. While more mechanistic than network inference, these methods cannot quantify the magnitude or even the sign of net interactions.

In this work, we fill these gaps by proposing a novel theoretical framework that enables a quantifiable, mechanistic representation of the dynamic linkage between microbial interactions and the environment. For this purpose, we synergistically integrate two complementary modeling frameworks to overcome their own limitations: a generalized Lotka-Volterra (gLV) model (29) and population growth kinetics. Like other network inference approaches, a typical gLV model with a focus on pairwise interactions is constructed based on an implicit assumption of constant

interactions. We relax this assumption by representing interaction coefficients in the gLV model as a function of environmental variables (i.e., concentrations of cross-fed metabolites and shared substrates) described in microbial growth kinetics, which is termed here kinetics-based inference of dynamic variation in microbial interactions (KIDI). The resulting functional representation of interactions by KIDI enables not only quantifying their dynamic variation as environmental conditions change, but also individually identifying negative and positive influences among species in mixed relationships. The prediction of KIDI was demonstrated accurate through a coordinated design of experiments using a binary consortium composed of tyrosine and tryptophan auxotrophic mutants of *Escherichia coli* (30) so that they both compete and/or cooperate depending on environmental conditions.

RESULTS

Formulation of a conceptual model for understanding environment-dependent interactions

For illustration of the concept of KIDI, we consider a hypothetical consortium composed of two members where species 1 (X_1) and species 2 (X_2) cooperate by cross-feeding S_1^+ and S_2^+ each other but compete for the shared metabolite S^- (the center circle in **Fig. 1**). Growth kinetics for the i^{th} species (X_i) (that requires two substrates S_i^+ and S^- for growth) can be represented, e.g., using a double Michaelis-Menten equation as follows:

$$\mu_i = \mu_i^{\max} \frac{s_i^+}{\left(K_i^+ + s_i^+\right)} \frac{s^-}{\left(K_i^- + s^-\right)}, \quad i = 1, 2 \tag{1}$$

where μ_i [1/h] is the specific growth rate of X_i, μ_i^{max} is the maximal specific growth rate, s_i^+ and s^- [g/l] are the concentrations of S_i^+ and S^-, and K_i^+ and K_i^- [g/l] are half-saturation constants associated with the consumption of S_i^+ and S^-, respectively. As inferable from growth kinetics in

Eq. (1), the mixed relationship (i.e., competition and cooperation) between X_1 and X_2 when both substrates are limiting can turn into diverse forms of interactions as environmental conditions change. When S^- is present in excess (therefore, no competition is necessary) but S_1^+ and S_2^+ are limiting, for example, their relationship is predominantly cooperative (where $\mu_i \approx \frac{\mu_i^{\max} s_i^+}{K_i^+ + s_i^+}$). As the opposite case, if both S_1^+ and S_2^+ are excessive in the environment (so no partners are needed to acquire them) while S^- is limiting, their relationship is governed by competition (where $\mu_i \approx \frac{\mu_i^{\max} s^-}{K_i^- + s^-}$). Likewise, one can assume many other different scenarios where their relationships turn into competition, cooperation, amensalism, commensalism and even neutrality, as illustrated in **Fig. 1**.

Representation of interaction parameters as a function of environmental variables

To model such environment-dependent microbial relationships, we derived a general form of interaction coefficients as a function of environmental variables by integrating growth kinetics and a gLV model. As described in detail in **Materials and Methods**, our formula (KIDI) represents interaction coefficients of species in the mixed relationship as a sum of positive and negative parts, i.e.,

$$a_{i,j}\left(s_i^+, s^-\right) = a_{i,j}^+\left(s_i^+, s^-\right) + a_{i,j}^-\left(s_i^+, s^-\right), \quad (i, j) = (1,2) \text{ or } (2,1) \tag{2}$$

where $a_{i,j}^+$ and $a_{i,j}^-$ denote the positive and negative influence of X_j on the growth rate of X_i, which are defined as follows:

$$a_{i,j}^+\left(s_i^+, s^-\right) \equiv \frac{\partial}{\partial s_i^+}\left[\mu_i\left(s_i^+, s^-\right)\right] \cdot \frac{\partial s_i^+}{\partial x_j} \tag{3}$$

$$a_{i,j}^{-}\left(s_i^{+},s^{-}\right)\equiv\frac{\partial}{\partial s^{-}}\left[\mu_i\left(s_i^{+},s^{-}\right)\right]\cdot\frac{\partial s^{-}}{\partial x_j} \tag{4}$$

The positive influence of X_j on the growth rate of X_i (i.e., $a_{i,j}^{+}$) is represented by the two subsequent terms on the right-hand side of Eq. (3): (i) the impact of the change in the population size of X_j on the concentration of the cross-fed substrate S_i^{+} (as denoted by $\partial s_i^{+}/\partial x_j$) and (2) the subsequent impact of the change in S_i^{+} on the growth rate of the i^{th} species (i.e., μ_i) (as denoted by $\partial[\mu_i(s^{-},s_i^{+})]/\partial s_i^{+}$). The negative impact of X_j on the growth rate of X_i ($a_{i,j}^{-}$) in Eq. (4) can be interpreted in a similar fashion.

The derivative terms on the right-hand side of Eqs. (3) and (4) are fully identifiable from reaction stoichiometry and kinetics. In the case of using a double Monod kinetics, for example, incorporation of Eq. (1) into Eqs. (3) and (4) yields $a_{i,j}^{+}$ and $a_{i,j}^{-}$ as follows:

$$a_{i,j}^{+}\left(s_i^{+},s^{-}\right)=\left[\mu_i^{\max}\frac{K_i^{+}}{\left(K_i^{+}+s_i^{+}\right)^2}\frac{s^{-}}{\left(K_i^{-}+s^{-}\right)}\right]\cdot Y_{S_i^{+}/X_j} \tag{5}$$

$$a_{i,j}^{-}\left(s_i^{+},s^{-}\right)=\left[\mu_i^{\max}\frac{s_i^{+}}{\left(K_i^{+}+s_i^{+}\right)}\frac{K_i^{-}}{\left(K_i^{-}+s^{-}\right)^2}\right]\cdot\left(-Y_{S^{-}/X_j}\right) \tag{6}$$

where $Y_{S_i^{+}/X_j}$ and Y_{S^{-}/X_j} denote the stoichiometric relationships between the changes in substrate and biomass concentrations associated with X_j, i.e., $Y_{S_i^{+}/X_j}=|\Delta s_i^{+}/\Delta x_j|$ and $Y_{S^{-}/X_j}=|\Delta s^{-}/\Delta x_j|$ (see **Materials and Methods**).

To identify net interactions between two species with mixed relationships, we further defined a universal interaction parameter $\gamma_{i,j}$ as follows:

$$\gamma_{i,j}\equiv\frac{a_{i,j}^{+}+a_{i,j}^{-}}{a_{i,j}^{+}-a_{i,j}^{-}},\quad (i,j)=(1,2)\text{ or }(2,1) \tag{7}$$

The parameter $\gamma_{i,j}$ ranges from -1 to 1 to represent positive influences of species j on species i when greater than 0 and negative impacts when less than 0, respectively, consequently allowing us to conveniently quantify the relative dominance of inhibition vs. promotion in mixed interactions. The parameter $\gamma_{i,j}$ complements $a_{i,j}$, rather than replaces it, in that the magnitude of interactions cannot be determined by $\gamma_{i,j}$, but by the original interaction parameter, $a_{i,j}$. Along with $a_{i,j}$ defined in Eqs. (2) to (4), $\gamma_{i,j}$ completely characterizes the dynamic variation of interactions between X_1 and X_2 based on co-culture growth data as demonstrated in the following sections.

Identification of kinetics and stoichiometry via data fit

For experimental demonstration of the mathematical formulation derived in the previous section, we constructed a synthetic consortium composed of two *E. coli* auxotrophic mutants that cooperatively cross-feed tryptophan and tyrosine, respectively, while competitively growing on glucose (31). This consortium is therefore an ideal, simplest model system for studying environment-dependent dynamic variations in microbial interactions. Due to its exact correspondence to the hypothetical consortium in **Fig. 1**, we denote two *E. coli* mutant strains ΔtrpC and ΔtyrA by X_1 and X_2; glucose, tryptophan, and tyrosine by S^-, S_1^+, and S_2^+, respectively.

Using these two strains, we performed growth experiments under diverse culture conditions: two individual batch experiments using X_1 (**Fig. 2A**) and X_2 (**Fig. 2B**), respectively, and two sets of co-culture experiments (**Figs. 2C** and **2D**). The top panels in **Figs. 2C** and **2D** denote co-growth experiments in batch cultures, while the middle and bottom panels denote semi-batch modes, where we added glucose feedbeads (FBs) at time 7.5 and 10 hours, respectively, to induce dramatic changes in interspecies interactions during co-growth. Other differences in co-

culture conditions in **Figs. 2C** and **2D** include initial concentrations of S^-, S_1^+, and S_2^+, and the number of added FBs (see **Supp Datasheet**). The optical density profiles in **Fig. 2D** denote the combined population change of both strains, i.e., $X_1 + X_2$.

Based on the four datasets in **Fig. 2**, we constructed a dynamic co-growth model of X_1 and X_2 to determine associated kinetics and stoichiometry, key information required for quantifying interspecies interactions parameters ($a_{i,j}$ and $\gamma_{i,j}$) in Eqs. (2) to (7). The dynamic co-growth model is composed of five mass balance equations for X_1, X_2, S^-, S_1^+, and S_2^+. We determined stochiometric and kinetic parameters using three subsets of data in **Figs. 2A – 2C** and validated the model against the remaining one (in **Fig. 2D**) that was not used for model identification. The robust consistency between simulated and measured data in **Fig. 2D**, as well as those in **Figs. 2A – 2C**, indicates the acceptability of using the identified model parameters in inferring interaction coefficients. We provide the full list of model equations with parameter values in **Table 1**; the culture conditions in **Table S1**.

Variation in microbial interactions driven by the switch in limiting substrates in batch cultures

Based on the stochiometric and kinetic parameters determined through data fit in **Table 1**, we were able to determine microbial interactions and their variations as a function of environmental conditions using KIDI. We first analyzed various co-culture scenarios in batch modes (**Fig. 3**). In **Fig. 3A**, we considered the growth of X_1 and X_2 on relatively high and low initial concentrations of S^- (2 g/l) and S_1^+ and S_2^+ (i.e., 0.4 mg/l for both) as a reference condition. As shown in the top two panels of **Fig. 3A**, S^- was depleted around 22.5 hours, after which no further microbial growth is observed for both X_1 and X_2. In the present setting, the initial relationship between X_1 and X_2 is

188 expected to be cooperative (because S^- is excessive in the beginning), which however turns into
189 competition as the level of S^- gradually decreases. Interaction coefficients extracted by KIDI
190 correctly captured this transition as indicated by the dramatic changes in the values of normalized
191 universal interaction parameters ($\gamma_{1,2}$ and $\gamma_{2,1}$) from 1 to -1 around the time when glucose is
192 depleted. Actual values of interaction coefficients can be seen from $a_{i,j}$, $a_{i,j}^+$, and $a_{i,j}^-$ (three bottom
193 panels of **Fig. 3A**, which also showed that the level of initial cooperation was moderate or small
194 (as indicated by small magnitudes of $a_{i,j}^+ < 2 \times 10^{-3}$), partly due to the availability of S_1^+ and S_2^+
195 in the environment from the beginning. Interestingly, the values of $a_{i,j}^+$ dropped to zero after the
196 depletion of S^- despite that the initially added S_1^+ and S_2^+ might be completely consumed by that
197 time and consequently metabolic dependence between X_1 and X_2 should increase. The reason for
198 zero values of $a_{i,j}^+$ is due to that the exchange of S_1^+ and S_2^+ is not occurring when species cannot
199 grow any more due to carbon limitation after the depletion of S^-.

200 For comparison, we analyzed two additional conditions. (1) with a lower initial
201 concentration of S^- (i.e., 0.5 g/l) and (2) with lower and higher initial concentrations of S^- (0.5
202 g/l) and S_1^+ and S_2^+ (i.e., 4 mg/l for both), respectively. In both cases, KIDI successfully captured
203 the expected changes in interspecies interactions. In the case of lowering the initial concentration
204 of S^- (**Fig. 3B**), KIDI showed that the level of initial competition increases (due to the limited
205 availability of S^-) as indicated by relatively lower values of $\gamma_{1,2}$ and $\gamma_{2,1}$ compared to the case of
206 **Fig. 3A**. Notably, $\gamma_{2,1}$ showed negative value throughout the co-growth (indicating the dominance
207 of negative influence of X_1 on the growth of X_2). In the case of increasing the initial concentrations
208 of S_1^+ and S_2^+ in addition to lowering S^- (**Fig. 3C**), the relationship between the two strains became
209 even more negative, which was also an expected outcome because metabolic dependence between

X_1 and X_2 will accordingly reduce when they can acquire what they need from the environment, rather than from partners.

In all three cases above (including the reference condition), the relations between the two *E. coli* strains were shown asymmetric, i.e., $\gamma_{1,2} \neq \gamma_{2,1}$, $a_{1,2} \neq a_{2,1}$, $a^-_{1,2} \neq a^-_{2,1}$, and $a^+_{1,2} \neq a^+_{2,1}$. Interestingly, KIDI consistently predicted $\gamma_{1,2} > \gamma_{2,1}$ and $a_{1,2} > a_{2,1}$, while the reasons may vary across conditions. In the reference condition (**Fig. 3A**) where glucose is excessive (so $a^-_{i,j}$'s are negligible), it is mostly due to $a^+_{1,2} > a^+_{2,1}$ (i.e., X_1 has a higher comparative advantage in exchanging amino acids with X_2 than the other way around) that leads $\gamma_{1,2} > \gamma_{2,1}$ (as well as $a_{1,2} > a_{2,1}$) (see **Fig. S1A** for a zoom-in view). In contrast, in the case in **Fig. 3C** where the glucose level is low while amino acids are abundant (so $a^+_{i,j}$'s are negligible), X_1 has the comparative growth advantage because $a^-_{1,2} > a^-_{2,1}$ (i.e., the growth of X_1 is less inhibited by X_2 than the other way around) (**Fig. S1C**). Lastly, both $a^+_{i,j}$'s and $a^-_{i,j}$'s contribute to the outcome in the case in **Fig. 3B** where all substrates (glucose and amino acids) are limitedly available in the environment (**Fig. S1B**).

Dynamic response of microbial interactions to environmental perturbations during growth

We extend our analysis to semi-batch cultures that are perturbed by the addition of glucose FBs during growth and therefore are expected to show more dramatic changes in interspecies interactions and community dynamics. In contrast with the batch cultures considered in the previous section where no further growth is possible after the depletion of the initially added S^-, the two strains continue to grow in semi-batch cultures due to slow but continual provision of S^- from the added FBs. Despite a general expectation that the competition level between the two strains will be mitigated at least at the moment of FB addition, it is uncertain: (1) to what degree

this will occur under different environmental conditions, and (2) how governing microbial interactions will shift (between competition and cooperation), particularly in a later phase when the growth of the two strains is be limited by both S^- and S_i^+. To answer these questions, we applied KIDI to the following three cases. For simplicity, we set the initial conditions to be the same as before.

First, we considered the initial concentrations of 2 g/l for S^- and 0.4 mg/l for S_1^+ and S_2^+ and added 3 FBs of S^- at around 7.5 hours (**Fig. 4A**). Due to the relatively high concentration of S^-, the impact of adding 3 FBs of S^- was minimal, i.e., showing no appreciable qualitative changes (in glucose concentration, population size, and interaction parameters) from the batch case with the same initial conditions in **Fig. 3A**. By contrast, when the initial concentration of S^- was low (i.e., 0.5 g/l) (**Fig. 4B**), KIDI identified the significant impact of adding FBs on both glucose concentration and microbial interactions, as indicated by sudden increases in S^-, $\gamma_{1,2}$ and $\gamma_{2,1}$. More interestingly, when additionally increasing the initial concentration of S_1^+ and S_2^+ (**Fig. 4C**) (therefore the level of competition becomes even more significant), we found no appreciable impacts on microbial interactions ($\gamma_{1,2}$ and $\gamma_{2,1}$), while the glucose (S^-) profile was significantly perturbed by adding FBs. As observed in the previous section, the *net* interaction parameters ($a_{i,j}$ and $\gamma_{i,j}$) are governed by $a_{i,j}^+$ and/or $a_{i,j}^-$ depending on the environmental contexts: $a_{i,j}^+$ and $a_{i,j}^-$ are major determinants of the net interaction for the cases in **Figs. 4A** and **4C**, respectively, while the effects of $a_{i,j}^+$ and $a_{i,j}^-$ are comparable for the case in **Fig. 4B** (see zoom-in views in **Fig. S2**). In all three cases, the interactions between the two strains were eventually governed by competition in the later phase as indicated by the negative values of $\gamma_{1,2}$ and $\gamma_{2,1}$ close to -1. However, governing interactions in the early phase depended on initial conditions, i.e., cooperation and competition were dominant in the first and third cases (**Figs. 4A** and **4C**), respectively, while the

second case (**Fig.4B**) showed a balance between them. Similar interpretations can be made for other scenarios of perturbations where the number of added FBs and the timing of addition were subject to variation (**Fig. S3**).

Interactions between X_1 and X_2 were also identified asymmetric. Similar to the previous batch cases, X_1 has the comparative advantage over X_2 throughout the entire growth period by being more helped from X_2 (than X_2 is being helped from X_1) (i.e., $a_{1,2}^{+} > a_{2,1}^{+}$) before the exhaustion of initially added S^{-}, and by being less inhibited by X_1 than X_2 is being inhibited by X_1 (i.e., $a_{1,2}^{-} < a_{2,1}^{-}$) afterwards.

DISCUSSION

In this study, we proposed a novel computational method (KIDI) that enables quantitatively identifying environment-dependent interspecies interactions in microbial communities. By integrating growth kinetics into a gLV model, we derived an analytical form of interaction coefficients as a function of environmental variables (i.e., concentrations of chemical substrates that affect interactions), the results of which were subsequently validated through a coordinated design of co-culture experiments.

Our theoretical development significantly extends the current scope of microbial ecological modeling by completely relaxing the typical assumption of constant interactions among species. The gLV model, for example, has been widely used as a basic ecological modeling template for simulation of population dynamics and inference of interspecies interactions in microbial communities (26-28). Due to the constant interaction assumption, however, the application of the gLV model is often confined to a narrow range of conditions where interspecies interactions are expected to remain largely constant. KIDI addresses this limitation by representing interaction

279 coefficients as an explicit function of limiting substrates. As an exception, a previous study by
280 Momeni et al. (32) showed that pairwise interaction (i.e., gLV) models are derivable from
281 mechanistic (i.e., kinetic) models through empirical manipulation of equations, which is however
282 limited to special forms of kinetics and therefore cannot be generalizable (32). By contrast, our
283 chain rule-based formulation allows us to handle any complex forms of kinetic equations with no
284 such constraints. Consequently, KIDI enables incorporation any forms of kinetic equations as
285 demonstrated using a double Michaelis-Menten kinetics as a demonstration example.

286 Dynamic variations in microbial interactions inferred by KIDI were experimentally
287 validated using a synthetic binary consortium of two metabolically engineered auxotrophic *E. coli*
288 mutants that cross-feed amino acids they cannot synthesize (i.e., tryptophane and tyrosine). A
289 coordinated design of experiments provided multiple sets of data required for determining kinetic
290 and stoichiometric parameters in the mechanistic model along with substrate concentrations, which
291 are key inputs for quantifying environment-dependent interactions. Despite diverse culture
292 conditions including axenic and binary growth in batch and semi-batch modes, our model with a
293 *single* set of parameters showed satisfactory fit to the three training datasets and provided
294 consistency with the validation dataset set aside in advance. Such a fair goodness of fit indicates
295 the acceptability of model parameters and therefore the subsequent inference of microbial
296 interactions.

297 Our kinetic model also shows consistency with the analysis of energetic cost of
298 synthesizing amino acids in the literature. Mee et al. (30) estimated the energetic cost for the
299 synthesis of 14 individual amino acids based the amounts of extracellularly supplemented amino
300 acid and the observed growth yield of *E. coli* auxotrophic mutants. From the linear relationships
301 between these two variables, they calculated the supplemented amounts of amino acids *per cell*,

which were 1.5×10^7 and 3.7×10^7 for the tryptophane and tyrosine auxotrophic *E. coli* mutants, respectively. These two quantities correspond to the stoichiometric coefficients $Y_{S_i^+/X_i}(i = 1,2)$ in our kinetic model, which were determined to be 0.0845 $(= Y_{S_1^+/X_1})$ and 0.133 $(= Y_{S_2^+/X_2})$ [mg/OD] through data fit (**Table 2**). As the direct one-to-one matching between them might not be feasible, e.g., due to different units of biomass (i.e., cell number in Mee et al. (30) vs. OD in this work), we compared the ratios, which showed consistency between the two studies, i.e., $\frac{1.5\times10^7}{3.7\times10^7} \approx 0.41$ vs. $\frac{0.0845}{0.133} \approx 0.64$. Both results imply that compared to tyrosine, the synthesis of tryptophane is more costly. In support of this, Mee et al. (30) estimated the biosynthetic cost for tryptophane is about 43% higher than that for tyrosine.

The formulation of KIDI is valid regardless of the complexity of microbial communities. A challenge exists, however, in accurately quantifying input parameters (i.e., kinetic and stoichiometric parameters of the kinetic model), because it requires robust measurements of temporal profiles of substrate concentrations. In particular, the levels of metabolites that are exchanged among member species are often quite low and sometimes below the detection limit due to immediate consumption after being produced. This difficulty would be relieved to a degree by performing axenic growth experiments (as we did in this work) but extracting isolates from natural communities may not be always possible. Under these constraints, our demonstration was focused on relatively simple consortia that facilitate to collect experimental data (temporal profiles of substrate concentrations and population densities) required to determine the parameters in the mechanistic model. In this regard, KIDI can serve as a valuable modeling tool for synthetic consortia designed for engineering applications and/or model consortia derived from natural communities to gain a better understanding of complex ecological systems (33, 34).

Despite this challenge, we highlight that inferring environment-dependent interactions and their dynamic variations is a critical capability uniquely associated with KIDI. Even in a simple binary consortium considered in this work, KIDI provides new insights into interspecies interactions such as asymmetry between the two amino acid autotrophs, which might not be obtainable otherwise. In perturbed growth experiments with glucose FBs, for example, KIDI identified that (1) $a_{1,2}^{+} > a_{2,1}^{+}$ while the shared substrate (glucose) is abundant, implying that the tryptophane auxotroph (X_1) does not support the growth of the tyrosine auxotroph (X_2) as much as X_2 does for X_1; (2) $a_{1,2}^{-} < a_{2,1}^{-}$ after the completion of initially added glucose, implying that less favorable supporters during cooperation become worse enemies when the relationship turned into competition. As another critical utility, KIDI can significantly facilitate the development of network inference techniques because the validation process of new algorithms for predicting microbial interactions has often been hampered due to the lack of benchmark data.

Beyond microbial ecology, KIDI is applicable in broad areas of community ecology because context dependency is not a property associated only with microorganisms, but with macro-organisms such as plants and animals. We hope that KIDI will serve as a useful tool for understanding and engineering context-dependent microbial interactions in a wide range of applications.

MATERIALS AND METHODS

Mathematical definition of interaction coefficients

The dynamic change in population i in a community can be formulated in a general form as follows:

$$\frac{1}{x_i}\frac{dx_i}{dt} = f_i\left(x_1, x_2, \cdots, x_N\right), \quad i = 1, 2, \cdots, N \tag{8}$$

where x_i is the population density of species i, the left-hand side defines a specific growth rate of species i (hereafter denoted by $\mu_i \equiv d(\ln x_i)/dt$), and the function $f_i(x_1, x_2, \cdots, x_N)$ represents a nonlinear dependence of μ_i on population densities of other species that affect the growth of species i.

Using a Taylor expansion, the right-hand side of Eq. (8) can be represented as a series of polynomial terms, i.e.,

$$\mu_i = f_{i,0} + \sum_{j=1}^{N} \left(\frac{\partial f_i}{\partial x_j} \right)_0 x_j + H.O.T., \quad i = 1, 2, \cdots, N \tag{9}$$

where the subscript 0 denotes a chosen reference condition, *H.O.T.* is higher-order terms. Neglecting the *H.O.T.* in Eq. (9), a gLV equation describes specific growth of species i using a linear equation, i.e.,

$$\mu_i \left(x_1, x_2, \cdots, x_N \right) = \mu_{i,0} + \sum_{j=1}^{N} a_{i,j} x_j, \quad i = 1, 2, \cdots, N \tag{10}$$

where interaction coefficient $a_{i,j}$ denotes the effect of species population j on the specific growth of species i. For a binary community, Eq. (10) reduces to

$$\mu_i \left(x_i, x_j \right) = \mu_{i,0} + a_{i,i} x_i + a_{i,j} x_j, \quad i = 1, 2 \tag{11}$$

where $\mu_{i,0}$ is the basal growth rate, $a_{i,i}$ is the intra-specific interaction coefficient, and $a_{i,j}$ is the inter-specific interaction coefficient.

From Eq. (11), binary interaction coefficients in gLV are defined as follows:

$$a_{i,j} \equiv \frac{\partial \mu_i \left(x_i, x_j \right)}{\partial x_j} \tag{12}$$

364 The gLV model assumes that $a_{i,j}$ is constant, which however leads the gLV model to fail to capture
365 delicate dynamics of microbial interactions. Indeed, $a_{i,j}$ is a dynamic parameter that changes its
366 value in varying environmental conditions as shown in the next section.
367
368 **Formulation of interaction coefficients as function of environmental variables**
369 Specific growth rates can also be kinetically represented as a function of nutrient concentrations
370 in the environment. In the circumstance considered in **Fig. 1**,

371 $$\mu_i = \mu_i\left(s_i^+, s^-\right) \tag{13}$$

372 where s_i^+ is the nutrient (such as Trp or Tyr) that species i needs to get either from its partner or
373 the environment, and s^- represents the shared nutrient (i.e., glucose) that two species compete for.
374 Based on the chain rule, we formulate $a_{i,j}$ as a function of nutrient concentrations by
375 plugging Eq. (13) into (12), i.e.,

376 $$\begin{aligned} a_{i,j} &= \frac{\partial}{\partial x_j}\left[\mu_i\left(s_i^+, s^-\right)\right] \\ &= \frac{\partial}{\partial s_i^+}\left[\mu_i\left(s_i^+, s^-\right)\right]\frac{\partial s_i^+}{\partial x_j} + \frac{\partial}{\partial s^-}\left[\mu_i\left(s_i^+, s^-\right)\right]\frac{\partial s^-}{\partial x_j} \end{aligned} \tag{14}$$

377 Note that the two terms on the R.H.S. of Eq. (14) represent the positive and negative effects of
378 species j on i through environmental variables, i.e., $a_{i,j}^+$ and $a_{i,j}^-$ as defined below

379 $$a_{i,j}^+ \equiv \frac{\partial}{\partial s_i^+}\left[\mu_i\left(s_i^+, s^-\right)\right]\frac{\partial s_i^+}{\partial x_j} \tag{15}$$

380 $$a_{i,j}^- \equiv \frac{\partial}{\partial s^-}\left[\mu_i\left(s_i^+, s^-\right)\right]\frac{\partial s^-}{\partial x_j} \tag{16}$$

381 In a similar fashion, we can formulate intra-specific interaction coefficients as functions of
382 environmental variables, i.e.,

383
$$a_{i,i} = \frac{\partial}{\partial x_i}\left[\mu_i\left(s_i^+, s^-\right)\right] = \frac{\partial}{\partial s_i^+}\left[\mu_i\left(s_i^+, s^-\right)\right]\frac{\partial s_i^+}{\partial x_i} + \frac{\partial}{\partial s^-}\left[\mu_i\left(s_i^+, s^-\right)\right]\frac{\partial s^-}{\partial x_i} \quad (17)$$

384 Final forms of $a_{i,j}(a_{i,j}^+$ and $a_{i,j}^-)$ and $a_{i,i}$ depend on specific kinetics for $\mu_i(s^-, s_i^+)$.

385

386 **Microorganisms and culture conditions**

387 Tyrsoine (Tyr) and Trptophan (Trp) auxotrophic *Escherichia coli* (*E.* coli) strains were purchased
388 from *E. coli* Genetic Stock Center (CGSC) at Yale University (http://cgsc2.biology.yale.edu/).
389 Each strain was incubated overnight at 37℃ and 225 rpm in 50 ml of Falcon tube containing 5 ml
390 of Lysogeny broth (LB) supplemented with 33 μg/l kanamycin. Culture cells were collected and
391 centrifuged them at 16,000 g, 4℃ for 1.5 min. The cell pellets were washed with K3 basal medium
392 to remove residual amino acids in the samples. The washed cells were resuspended and transferred
393 to 150 ml flasks carrying 25 ml of K3 defined minimal medium (5) containing glucose and 33 μg/l
394 kanamycin, and cultivated at 37℃ and 225 rpm. An initial absorbance at 600 nm (OD 600) was
395 0.04 with equivalent cell ratio. For batch mode, 4.5 g/l glucose was supplied in the culture medium.
396 For the fed-batch mode, 0.5 g/l of an initial glucose concentration was used to shorten the lag phase
397 and 3 or 5 glucose FeedBeads (Kühner, Basel, Switzerland), releasing glucose at constant rate,
398 were added when OD 600 reached 0.2. We collected 500 ul of culture medium from each flask
399 and centrifuged them at 16,000 g for 1.5 min. The supernatant and pellets were stored at -20℃
400 until further analysis.

401

402 **Analysis of glucose concentration in the culture medium**

403 The concentration of glucose was analyzed by a high-performance liquid chromatography (HPLC)
404 system (Agilent, Santa Ciara, CA) equipped with a 1260 refractive index detector (RID) and an
405 Aminex HPX-87H column (Bio-Rad, Hercules, CA). Five microliter of filtered supernatants were
406 injected. Analytes were separated isocratically using 5 mM sulfuric acid at a flow rate of 0.7
407 ml/min.
408
409 **Analysis of amino acids concentration in the culture medium**
410 The amino acids in 10 µl of filtered supernatants were analyzed using a ultra-performance liquid
411 chromatography (UPLC) (Waters, Milford, MA) coupled with a micrOTOF II mass spectrometry
412 (TOF-MS) system (Bruker, Bremen, Germany). Analytes were measured using a tunable UV
413 detector at 210 and 397 nm. The amino acids were separated by an Agilent Poroshell 120 EC-C18
414 column at 30℃. The 1 % (v/v) of formic acid in water (mobile phase A) and 1 % (v/v) of formic
415 acid in acetonitrile (mobile phase B) were used, respectively. The amino acids separation was
416 obtained at a flow rate of 0.3 ml/min with a gradient program that allowed 100% of mobile phase
417 A until 2.1 min followed by increasing mobile phase B to 40% for 2 min and then equilibrated at
418 0% of eluent B in a total analysis time of 6 min. Analysis of the amino acids was performed using
419 electrospray ionization (ESI) and full-scan TOF-MS spectra (50 - 650 m/z) with 500 V end plate
420 voltage and 4.5 kV capillary voltage. Nebulizer gas and drying gas were supplied in 1.8 bar and 8
421 ml/min, respectively. The dry temperature was kept at 220℃.
422
423 **Quantification of cell ratio in microbial consortium**
424 Quantitative PCR (qPCR) was carried out in a 96-well plate by using a CFX96 Real-Time
425 Detection System (Bio-Rad, Hercules, CA, USA). The pellets were resuspended in ultra-pure

426 water to make consistent concentration (OD600 = 0.4) and then, the 200 µl solution was transferred
427 to a 250 µl PCR tube. The solutions were incubated at 98℃ for 10 min for cell disruption using a
428 T100 Thermal Cycler (Bio-Rad). The lysed cells were transferred to 1.5 ml of tubes and
429 centrifuged at 20, 000 x g for 2 min. The supernatants were analyzed by qPCR. The qPCR mixture
430 was composed as follows: 3 µl of 10X Xtensa® buffer, 0.3 µl of primer mix (50 uM for each),
431 0.15 µl of i-Taq (i-DNA Biotechnology, Singapore), 3 µl of 25 mM $MgCl_2$, 5 µl of purified cell
432 lysate, and 18.55 µl of ultra-pure water. The thermal cycling was programmed as follows: 95℃
433 for 1 min and 30 cycles of (95℃ for 20 sec, 55℃ for 20 sec, 68℃ for 40 sec). The primers for
434 qPCR analysis to quantify the different *E. coli* strains were provided in **Table S3**. The qPCR
435 analysis was performed in triplicate for each sample.
436

437 **ACKNOWLEDGMENTS**

438 This work was supported by the National Research Foundation of Korea (NRF) grant funded by
439 the Korea government (MSIT) (No. 2020R1A2C2007192), and the Korea Institute of Planning
440 and Evaluation for Technology in Food, Agriculture, Forestry and Fisheries (iPET) funded by the
441 MAFRA (32136-05-1- HD050). This work was also partially supported from Nebraska Tobacco
442 Settlement Biomedical Research Enhancement Funds to H-SS.
443

444 **References**

445 1. Sorboni SG, Moghaddam HS, Jafarzadeh-Esfehani R, Soleimanpour S. 2022. A
446 Comprehensive Review on the Role of the Gut Microbiome in Human Neurological
447 Disorders. Clinical Microbiology Reviews 35.

2. Vijay A, Valdes AM. 2022. Role of the gut microbiome in chronic diseases: a narrative review. European Journal of Clinical Nutrition 76:489-501.

3. Sokol NW, Slessarev E, Marschmann GL, Nicolas A, Blazewicz SJ, Brodie EL, Firestone MK, Foley MM, Hestrin R, Hungate BA, Koch BJ, Stone BW, Sullivan MB, Zablocki O, Pett-Ridge J, Consortium LSM. 2022. Life and death in the soil microbiome: how ecological processes influence biogeochemistry. Nature Reviews Microbiology 20:415-430.

4. Trivedi P, Batista BD, Bazany KE, Singh BK. 2022. Plant-microbiome interactions under a changing world: responses, consequences and perspectives. New Phytologist 234:1951-1959.

5. Albright MBN, Louca S, Winkler DE, Feeser KL, Haig SJ, Whiteson KL, Emerson JB, Dunbar J. 2022. Solutions in microbiome engineering: prioritizing barriers to organism establishment. Isme Journal 16:331-338.

6. Konopka A, Lindemann S, Fredrickson J. 2015. Dynamics in microbial communities: unraveling mechanisms to identify principles. Isme Journal 9:1488-1495.

7. Marsh JW, Ley RE. 2022. Microbiome engineering: Taming the untractable. Cell 185:416-418.

8. Perez-Garcia O, Lear G, Singhal N. 2016. Metabolic Network Modeling of Microbial Interactions in Natural and Engineered Environmental Systems. Frontiers in Microbiology 7.

9. Allen BH, Gupta N, Edirisinghe JN, Faria JP, Henry CS. 2022. Application of the metabolic modeling pipeline in KBase to categorize reactions, predict essential genes,

and predict pathways in an isolate genome, p 291-320, Microbial Systems Biology. Springer.

10. Song H-S, Nelson WC, Lee J-Y, Taylor RC, Henry CS, Beliaev AS, Ramkrishna D, Bernstein HC. 2018. Metabolic network modeling for computer-aided design of microbial interactions.

11. Kessell AK, McCullough HC, Auchtung JM, Bernstein HC, Song HS. 2020. Predictive interactome modeling for precision microbiome engineering. Current Opinion in Chemical Engineering 30:77-85.

12. Song HS, Lindemann SR, Lee DY. 2021. Editorial: Predictive Modeling of Human Microbiota and Their Role in Health and Disease. Frontiers in Microbiology 12.

13. Choi YM, Lee YQ, Song HS, Lee DY. 2020. Genome scale metabolic models and analysis for evaluating probiotic potentials. Biochemical Society Transactions 48:1309-1321.

14. Song HS. 2018. Design Principles of Microbial Communities: From Understanding to Engineering. Current Genomics 19:699-700.

15. Lee JY, Haruta S, Kato S, Bernstein HC, Lindemann SR, Lee DY, Fredrickson JK, Song HS. 2020. Prediction of Neighbor-Dependent Microbial Interactions From Limited Population Data. Frontiers in Microbiology 10.

16. Song HS, Lee JY, Haruta S, Nelson WC, Lee DY, Lindemann SR, Fredrickson JK, Bernstein HC. 2019. Minimal Interspecies Interaction Adjustment (MIIA): Inference of Neighbor-Dependent Interactions in Microbial Communities. Frontiers in Microbiology 10.

17. Kato S, Haruta S, Cui ZJ, Ishii M, Igarashi Y. 2008. Network relationships of bacteria in a stable mixed culture. Microbial Ecology 56:403-411.

18. Yamamoto K, Haruta S, Kato S, Ishii M, Igarashi Y. 2010. Determinative Factors of Competitive Advantage between Aerobic Bacteria for Niches at the Air-Liquid Interface. Microbes and Environments 25:317-320.

19. Klitgord N, Segre D. 2010. Environments that Induce Synthetic Microbial Ecosystems. Plos Computational Biology 6.

20. Song H-S, Cannon WR, Beliaev AS, Konopka A. 2014. Mathematical modeling of microbial community dynamics: a methodological review. Processes 2:711-752.

21. Faust K, Raes J. 2012. Microbial interactions: from networks to models. Nature Reviews Microbiology 10:538-550.

22. Friedman J, Alm EJ. 2012. Inferring Correlation Networks from Genomic Survey Data. Plos Computational Biology 8.

23. Fang HY, Huang CC, Zhao HY, Deng MH. 2015. CCLasso: correlation inference for compositional data through Lasso. Bioinformatics 31:3172-3180.

24. Ban YG, An LL, Jiang HM. 2015. Investigating microbial co-occurrence patterns based on metagenomic compositional data. Bioinformatics 31:3322-3329.

25. Joseph TA, Shenhav L, Xavier JB, Halperin E, Peer I. 2020. Compositional Lotka-Volterra describes microbial dynamics in the simplex. Plos Computational Biology 16.

26. Fisher CK, Mehta P. 2014. Identifying Keystone Species in the Human Gut Microbiome from Metagenomic Timeseries Using Sparse Linear Regression. Plos One 9.

513 27. Stein RR, Bucci V, Toussaint NC, Buffie CG, Ratsch G, Pamer EG, Sander C, Xavier JB.
514 2013. Ecological Modeling from Time-Series Inference: Insight into Dynamics and
515 Stability of Intestinal Microbiota. Plos Computational Biology 9.
516 28. Li CH, Chng KR, Kwah JS, Av-Shalom TV, Tucker-Kellogg L, Nagarajan N. 2019. An
517 expectation-maximization algorithm enables accurate ecological modeling using
518 longitudinal microbiome sequencing data. Microbiome 7.
519 29. Saeedian M, Pigani E, Maritan A, Suweis S, Azaele S. 2022. Effect of delay on the
520 emergent stability patterns in generalized Lotka-Volterra ecological dynamics.
521 Philosophical Transactions of the Royal Society a-Mathematical Physical and
522 Engineering Sciences 380.
523 30. Mee MT, Collins JJ, Church GM, Wang HH. 2014. Syntrophic exchange in synthetic
524 microbial communities. Proceedings of the National Academy of Sciences of the United
525 States of America 111:E2149-E2156.
526 31. Kerner A, Park J, Williams A, Lin XXNN. 2012. A Programmable Escherichia coli
527 Consortium via Tunable Symbiosis. Plos One 7.
528 32. Momeni B, Xie L, Shou WY. 2017. Lotka-Volterra pairwise modeling fails to capture
529 diverse pairwise microbial interactions. Elife 6.
530 33. McClure R, Naylor D, Farris Y, Davison M, Fansler SJ, Hofmockel KS, Jansson JK.
531 2020. Development and Analysis of a Stable, Reduced Complexity Model Soil
532 Microbiome. Frontiers in Microbiology 11.
533 34. Kylilis N, Tuza ZA, Stan GB, Polizzi KM. 2018. Tools for engineering coordinated
534 system behaviour in synthetic microbial consortia. Nature Communications 9.
535
536

Table captions

Table 1. Model equations with kinetic parameters and stoichiometric coefficients determined through the model fit to experimental data collected under various limiting conditions. R_i is the stoichiometric growth reaction for X_i, and Y_{S^-/X_i}, $Y_{S_i^+/X_i}$, and $Y_{S_j^+/X_i}$ denote the stoichiometric coefficients for S^-, S_i^+, and S_j^+ associated with the growth of X_i. s^-, s_i^+, and s_j^+ respectively denote concentrations of S^-, S_i^+, and S_j^+, x_i is the population density of X_i, μ_i is the specific growth rate of X_i, $k_{d,i}$ is the death rate of X_i, and q_{s^-} is the substrate releasing rate from FBs in glucose-limited semi-batch cultures (i.e., $q_{s^-} = 0$ in a batch mode). μ_i^{max} is the maximal growth rate, and K_i^- and K_i^+ are half-saturation constants associated with the consumption of S^- and S_i^+.

548 **Figure captions**

549 **Fig. 1.** Conceptual illustration of context-dependent microbial interactions in a binary
550 consortium dictated by the environmental contexts. Two species X_1 and X_2 compete for the
551 substrate S^- but cooperate by cross-feeding metabolite S_1^+ and S_2^+ (center panel). This mixed
552 relationship between X_1 and X_2 diverge into six different types of interactions by excessive
553 addition of specific substrates S_1^+, S_2^+, and/or S^-. Symbols next to the arrows denote the
554 substrate(s) excessively added to the environment. (**c**) Model microbial consortium using
555 tyrosine or tryptophan auxotrophic E. coli strains. Glucose is sole carbon source for both *E. coli*
556 strains. GLC, Tyr and Trp denote glucose, tyrosine, and tryptophan, respectively.
557
558 **Fig. 2.** Experimental data and model simulations for the growth of two *E. coli* mutant strains in
559 axenic and binary culture conditions: **A** and **B** are cultures of Trp auxotrophic and Tyr
560 auxotrophic *E. coli* mutants (X_1 and X_2), respectively; **C** and **D** are co-cultures with two
561 auxotrophs in batch and semi-batch cultures. Detailed culture conditions for the twelve panels
562 are provided in **Table S2**. Circles and lines denote the experimentally measured values and
563 simulation results, respectively. Black line denotes simulation results for glucose concentration
564 (S^-), and the lines in blue, red, and purple are simulated population densities of X_1, X_2, and $X_1 +$
565 X_2. **Figs. A, B,** and **C** show data fitting to determine model parameters, while the results in **Fig.**
566 **D** validate model predictions.
567
568 **Fig. 3**. Inference of dynamic variations of interaction parameters ($\gamma_{i,j}$, $a_{i,j}$, $a_{i,j}^+$, and $a_{i,j}^-$) for the
569 two *E. coli* mutants (X_1 and X_2) co-growing in three batch cultures: **A.** initial substrate
570 concentrations of 2 g/l glucose and 0.4 mg/l Trp & Tyr; **B.** initial substrate concentrations of 0.5

571 g/l glucose and 0.4 mg/l Trp & Tyr; and **C.** initial substrate concentrations of 0.5 g/l glucose and
572 4 mg/l Trp & Tyr. Black line denotes simulated glucose concentration (S^-); the lines in blue and
573 red indicate the variables and parameters associated with X_1 and X_2, respectively.

574

575 **Fig. 4**. Inference of dynamic variations of interaction parameters ($\gamma_{i,j}$, $a_{i,j}$, $a_{i,j}^+$, and $a_{i,j}^-$) for the
576 two *E. coli* mutants (X_1 and X_2) co-growing in three semi-batch cultures: **A.** initial substrate
577 concentrations of 2 g/l glucose and 0.4 mg/l Trp & Tyr, and 3 FBs added at 7.5 hours; **B.** initial
578 substrate concentrations of 0.5 g/l glucose and 0.4 mg/l Trp & Tyr, and 3 FBs added at 7.5 hours;
579 and **C.** initial substrate concentrations of 0.5 g/l glucose and 4 mg/l Trp & Tyr, and 3 FBs added
580 at 7.5 hours. Black line denotes simulated glucose concentration (S^-); the lines in blue and red
581 indicate the variables and parameters associated with X_1 and X_2, respectively.

582

583

584

585 Table 1
586

Stoichiometric equation (R_i) for growth of X_i:

$$\mathrm{R_i}: Y_{S^-/X_i}\mathrm{S^-} + Y_{S_i^+/X_i}\mathrm{S_i^+} \rightarrow \mathrm{X_i} + Y_{S_j^+/X_i}\mathrm{S_j^+}, \quad (i,j) = (1,2) \text{ or } (2,1) \tag{T1}$$

Dynamic mass balances:

$$\frac{dx_i}{dt} = \mu_i x_i - k_{d,i} x_i, \quad i = 1,2 \tag{T2}$$

$$\frac{ds^-}{dt} = -Y_{S^-/X_1}\mu_1 x_1 - Y_{S^-/X_2}\mu_2 x_2 (+q_{S^-}) \tag{T3}$$

$$\frac{ds_i^+}{dt} = -Y_{S_i^+/X_i}\mu_i x_i + Y_{S_i^+/X_j}\mu_j x_j, \quad (i,j) = (1,2) \text{ or } (2,1) \tag{T4}$$

Double Monod kinetics:

$$\mu_i = \mu_i^{\max} \frac{s_i^+}{(K_i^+ + s_i^+)} \frac{s^-}{(K_i^- + s^-)}, \quad i = 1,2 \tag{T5}$$

Kinetic parameters and stoichiometric coefficients determined through data fit:

Parameter	Value	Parameter	Value
$\mu_1^{\max}$ [1/h]	0.297	Y_{S^-/X_1} [g/OD]	1.26
$\mu_2^{\max}$ [1/h]	0.173	Y_{S^-/X_2} [g/OD]	1.47
K_1^- [g/l]	3.95 x 10^{-4}	$Y_{S_1^+/X_1}$ [mg/OD]	8.45 x 10^{-2}
K_2^- [g/l]	1.16 x 10^{-3}	$Y_{S_2^+/X_1}$ [mg/OD]	9.10 x 10^{-3}
K_1^+ [mg/l]	0.165	$Y_{S_1^+/X_2}$ [mg/OD]	0.107
K_2^+ [mg/l]	5.85 x 10^{-3}	$Y_{S_2^+/X_2}$ [mg/OD]	0.133
$k_{d,1}$ [1/h]	3.06 x 10^{-3}	q_{S^-} (for 3 FBs) [g/l/h]	4.80 X 10^{-2}
$k_{d,2}$ [1/h]	9.76 x 10^{-4}	q_{S^-} (for 5 FBs) [g/l/h]	8.01 x 10^{-2}

587

588

589 Figure 1

590

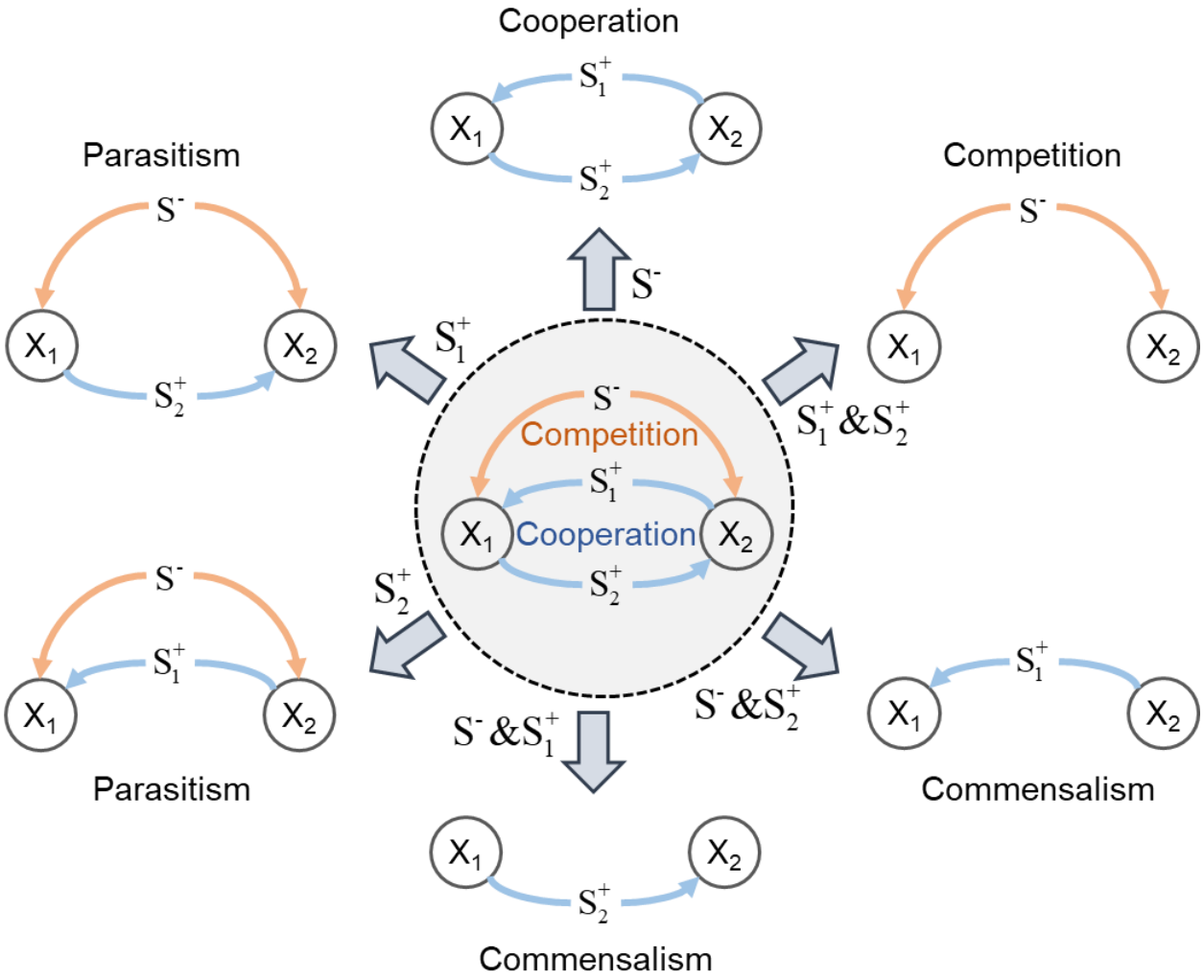

591

592

593

Figure 2

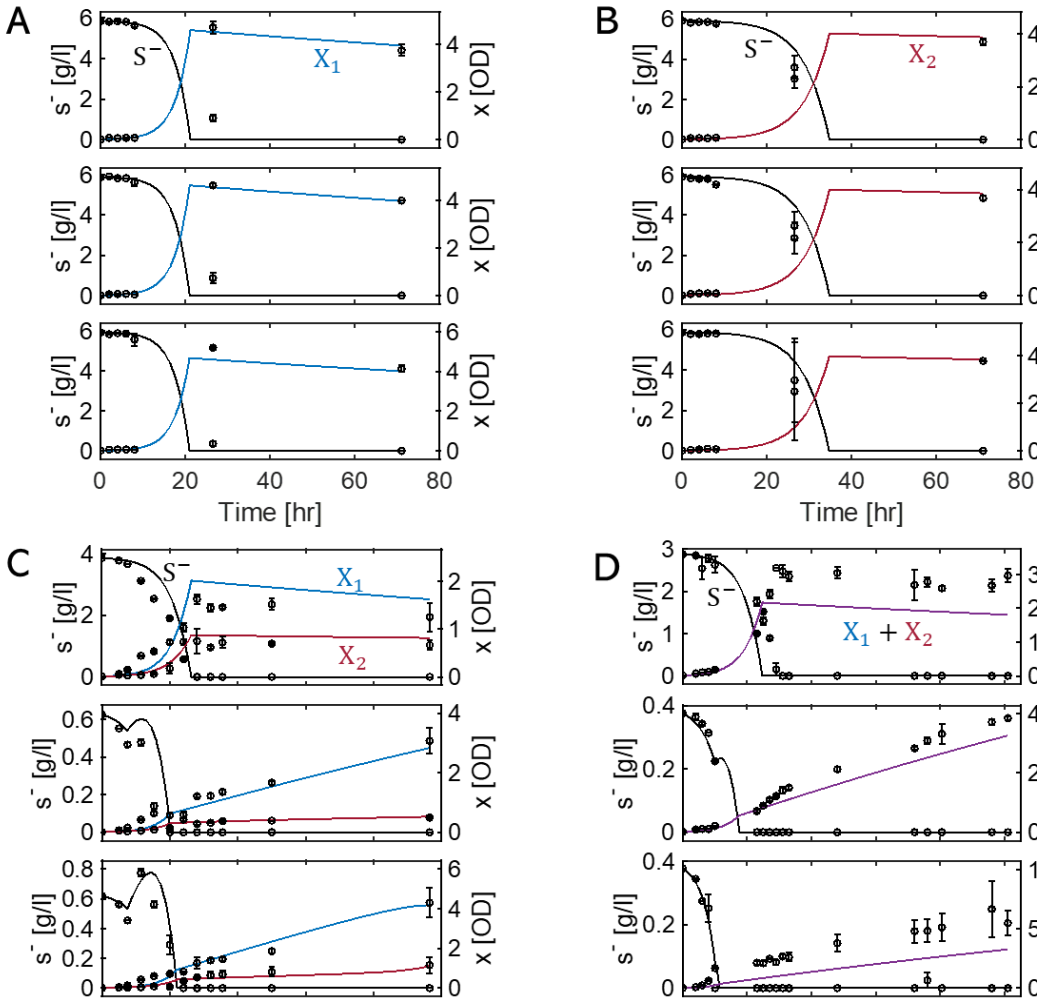

598 Figure 3

599

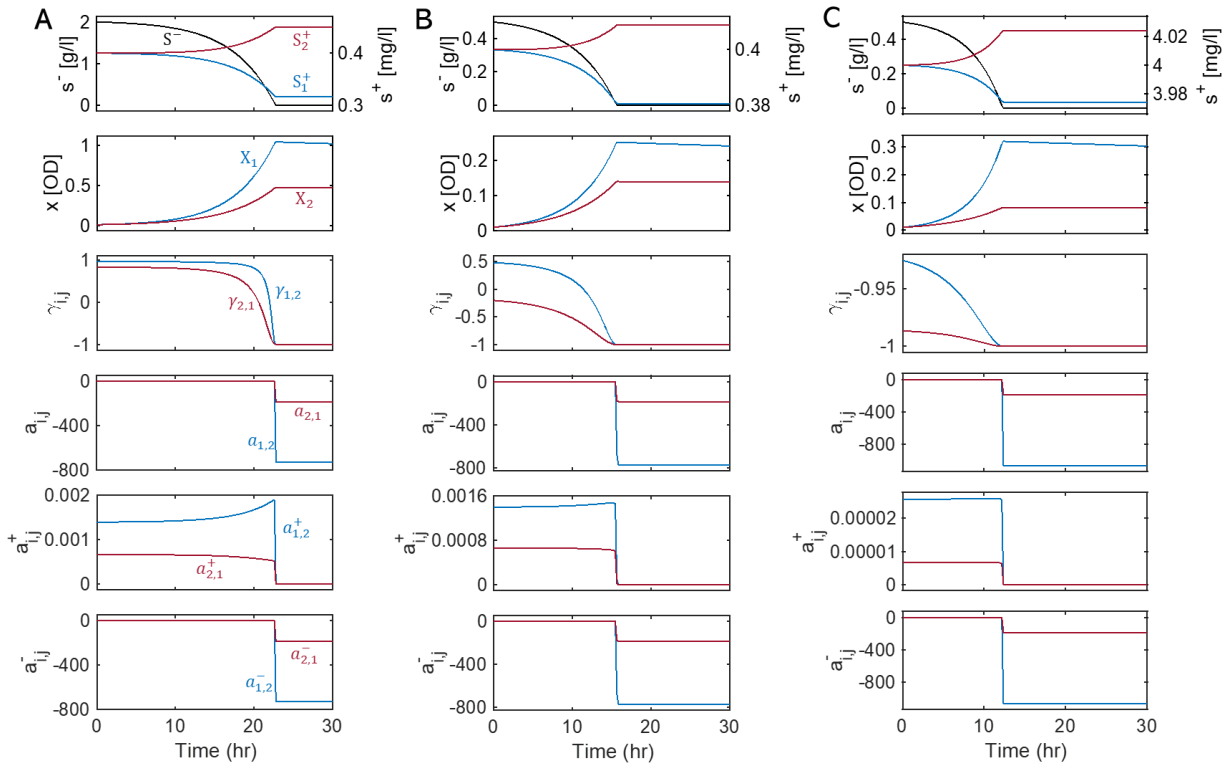

600

601

602 Figure 4

603

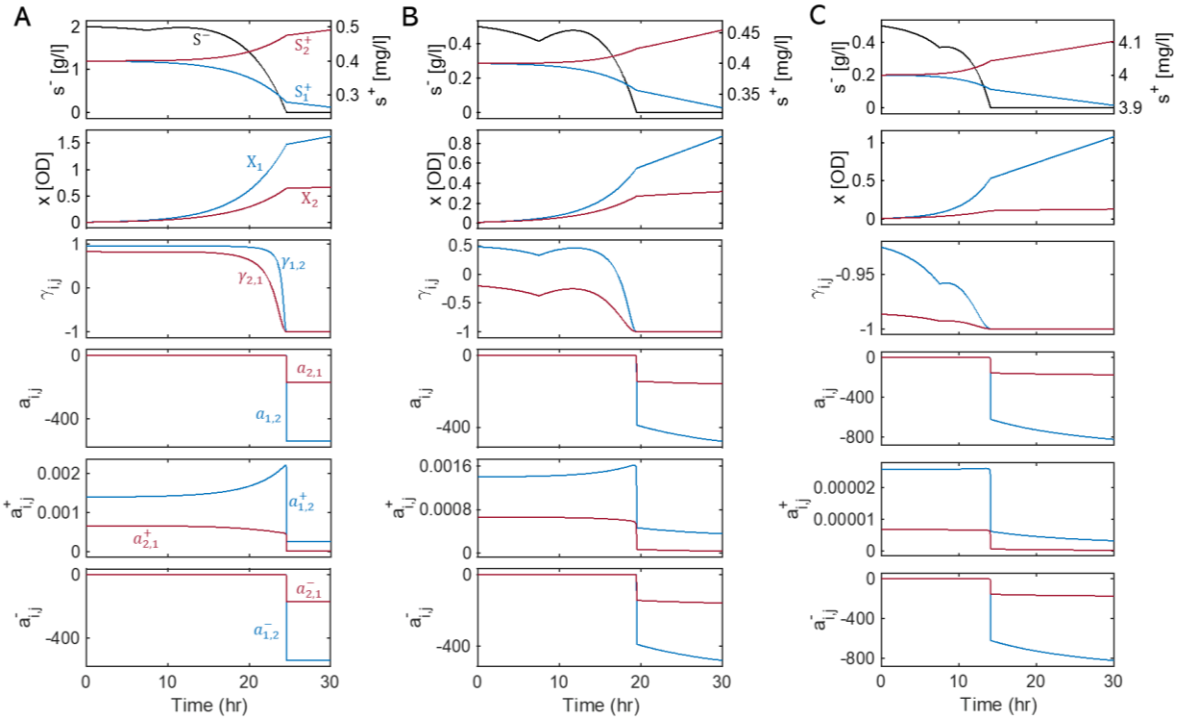

604

605

606 # SUPPLEMENTARY TABLES AND FIGURES

607

608 **Table S1.** Initial culture conditions for experimental data displayed in Fig. 2.

609

Exp #	Corresponding figures	Initial inoculum size (OD)	Glucose (mg/l)	Tryptophan (mg/l)	Tyrosine (mg/l)	# of FBs added	Time FBs added (hr)
1	Fig. 2A (top panel)	ΔTrp only: 0.01	5.838	10	-	-	-
2	Fig. 2A (middle panel)	ΔTrp only: 0.01	5.870	20	-	-	-
3	Fig. 2A (bottom panel)	ΔTrp only: 0.01	5.936	40	-	-	-
4	Fig. 2B (top panel)	ΔTyr only: 0.01	5.920	-	10	-	-
5	Fig. 2B (middle panel)	ΔTyr only: 0.01	5.909	-	20	-	-
6	Fig. 2B (bottom panel)	ΔTyr only: 0.01	5.863	-	40	-	-
7	Fig. 2C (top panel)	ΔTrp: 0.01 ΔTyr: 0.01	3.851	0.4	0.4	-	-
8	Fig. 2C (middle panel)	ΔTrp: 0.01 ΔTyr: 0.01	0.626	0.4	0.4	3	7.5
9	Fig. 2C (bottom panel)	ΔTrp: 0.01 ΔTyr: 0.01	0.620	0.4	0.4	5	7.5
10	Fig. 2D (top panel)	ΔTrp: 0.01 ΔTyr: 0.01	2.878	0.4	0.4	-	-
11	Fig. 2D (middle panel)	ΔTrp: 0.01 ΔTyr: 0.01	0.375	0.4	0.4	3	10
12	Fig. 2D (bottom panel)	ΔTrp: 0.01 ΔTyr: 0.01	0.377	200	200	3	10

610

611

612 **Table S2.** Sequence of the primers used in the qPCR analysis.

613

Primer	Sequence
Trp F	GCCGATGCCTGCTTATTA
Trp R	GCTCCTGTTCCTCTTCAT
Tyr F	CATTATGTCGTCAGAGCG
Tyr R	CCTTGCGGAAACTGTCAA

614
615

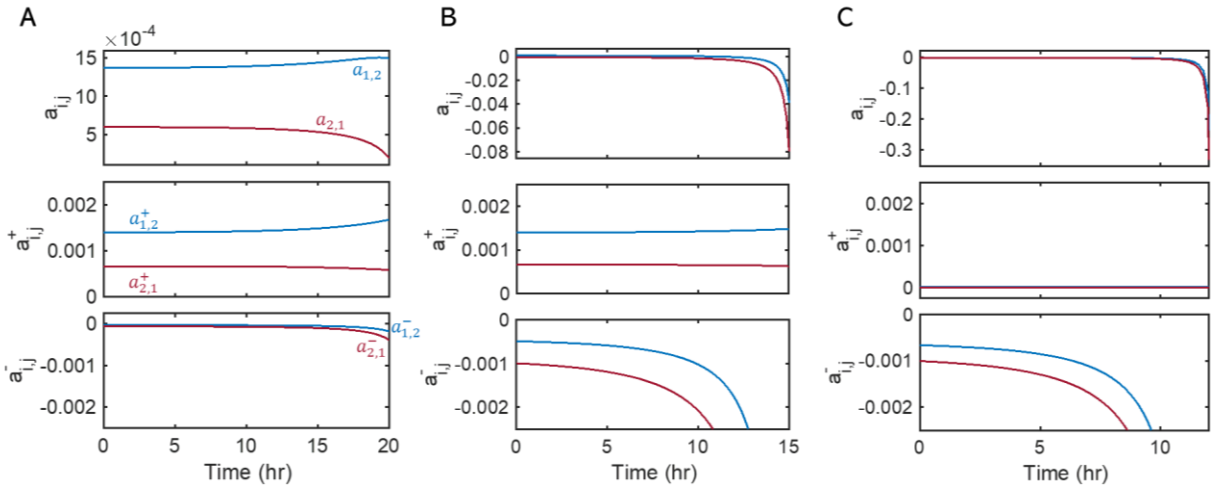

Figure S1. Zoom-in views of in interaction parameters, $a_{i,j}$, $a_{i,j}^{+}$, and $a_{i,j}^{-}$ in **Figs. 3A, 3B, and 3C,** respectively. The color scheme is the same as in **Fig. 3**.

622

623

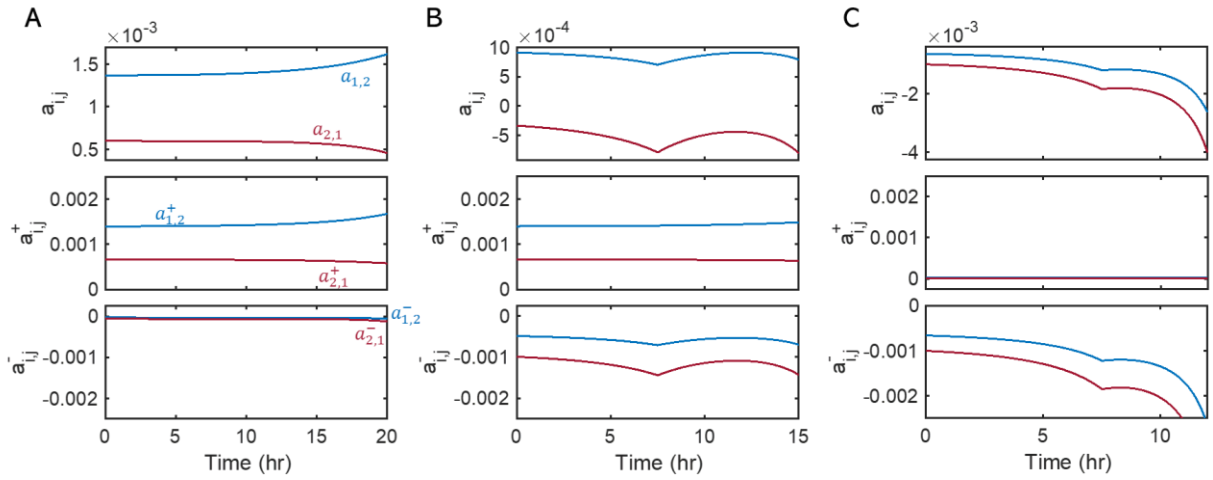

624

625 **Figure S2.** Zoom-in views of in interaction parameters, $a_{i,j}$, $a^{+}_{i,j}$, and $a^{-}_{i,j}$ in **Figs. 4A, 4B, and**
626 **4C,** respectively. The color scheme is the same as in **Fig. 4**.

627

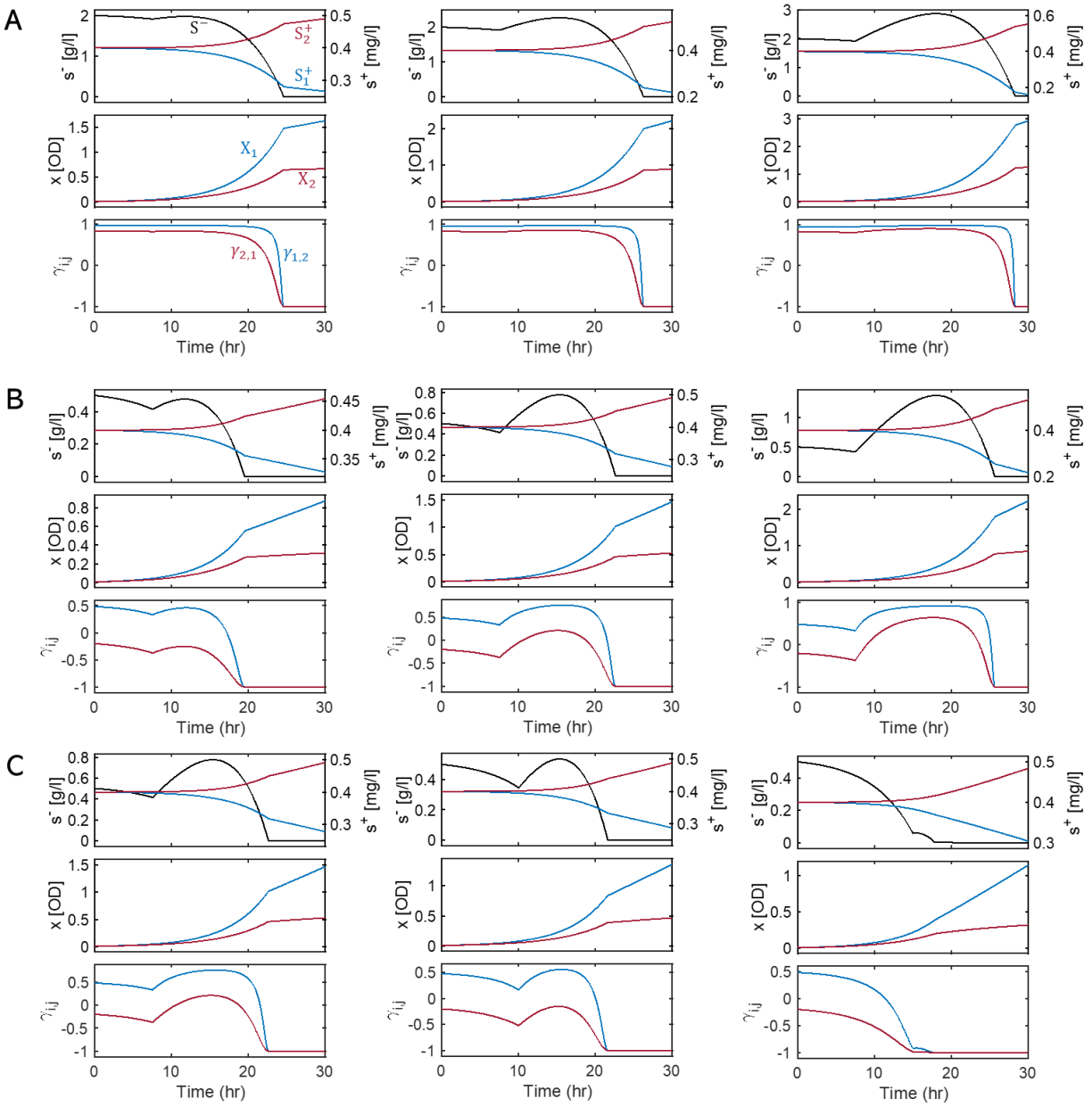

Figure S3. The predicted impacts of the numbers and timings of added FBs on the substrate profile (S^-), the population dynamics (X_1 and X_2), and the interaction parameter ($\gamma_{i,j}$): **A.** initial substrate concentrations of 2 g/l glucose and 0.4 mg/l Trp & Tyr with 3 FBs (left), 6 FBs (middle) and 10 FBs (right) added at 7.5 hours; **B.** initial substrate concentrations of 0.5 g/l glucose and 0.4 mg/l Trp & Tyr with 3 FBs (left), 6 FBs (middle) and 10 FBs (right) added at 7.5 hours; and **C.** initial substrate concentrations of 0.5 g/l glucose and 4 mg/l Trp & Tyr, with 6 FBs added at 7.5 hours (left), 10 hours (middle) and 15 hours (right). The color scheme is the same as **Fig. 4**.